Chemical Process Technology Department
Chemical Technology Section

WSRC-TR-94-0437
Revision 1

Keywords: H Canyon
TBP Oxidation
Mixing
Bubbling
Two-Layer

Retention : Permanent

Classification: U

James E Laurinat
Authorized Derivative Classifier

Mass Transfer Model for Two-Layer TBP Oxidation Reactions (U)

November 4, 1994

Westinghouse Savannah River Company
P. O. Box 616
Aiken, SC 29802

Prepared by the U. S. Department of Energy under Contract DE-AC09-89SR18035

DISCLAIMER

DISCLAIMER

Portions of this document may be illegible in electronic image products. Images are produced from the best available original document.

Chemical Process Technology Department
Chemical Technology Section

WSRC-TR-94-0437
Revision 1

Mass Transfer Model for Two-Layer TBP Oxidation Reactions (U)

By

J. E. Laurinat

Issued: November 4, 1994

Approvals

James E Laurinat 11-4-94

J. E. Laurinat, Author, CPT/C&HTS Date

N. M. Askew 11-4-94

N. M. Askew, Technical Reviewer Date

8 NOV 94

G. T. Geiger, Technical Reviewer Date

F. R. Graham 11/10/94

F. R. Graham, Responsible Manager, CPT/C&HTS Date

Table of Contents

1.0 Introduction

To prove that two-layer, TBP-nitric acid mixtures can be safely stored in the canyon evaporators, it must be demonstrated that a runaway reaction between TBP and nitric acid will not occur. Previous bench-scale experiments showed that, at typical evaporator temperatures, this reaction is endothermic and therefore cannot run away, due to the loss of heat from evaporation of water in the organic layer [1]. However, the reaction would be exothermic and could run away if the small amount of water in the organic layer evaporates before the nitric acid in this layer is consumed by the reaction. Provided that there is enough water in the aqueous layer, this would occur if the organic layer is sufficiently thick so that the rate of loss of water by evaporation exceeds the rate of replenishment due to mixing with the aqueous layer.

Bubbles containing reaction products enhance the rate of transfer of water from the aqueous layer to the organic layer. These bubbles are generated by the oxidation of TBP and its reaction products in the organic layer and by the oxidation of butanol in the aqueous layer. Butanol is formed by the hydrolysis of TBP in the organic layer. For aqueous-layer bubbling to occur, butanol must transfer into the aqueous layer. Consequently, the rate of oxidation and bubble generation in the aqueous layer strongly depends on the rate of transfer of butanol from the organic to the aqueous layer.

This report presents measurements of mass transfer rates for the mixing of water and butanol in two-layer, TBP-aqueous mixtures, where the top layer is primarily TBP and the bottom layer is comprised of water or aqueous salt solution. Mass transfer coefficients are derived for use in the modeling of two-layer TBP-nitric acid oxidation experiments [1].

Three cases were investigated: 1) transfer of water into the TBP layer with sparging of both the aqueous and TBP layers, 2) transfer of water into the TBP layer with sparging of just the TBP layer, and 3) transfer of butanol into the aqueous layer with sparging of both layers. The TBP layer was comprised of 99% pure TBP (spiked with butanol for the butanol transfer experiments), and the aqueous layer was comprised of either water or an aluminum nitrate solution.

The liquid layers were air sparged to simulate the mixing due to the evolution of gases generated by oxidation reactions. A plastic tube and a glass frit sparger were used to provide different size bubbles. Rates of mass transfer were measured using infrared spectrophotometers provided by SRTC/Analytical Development.

2.0 Summary of Results

When both liquid layers were sparged, water mixed in the bottom 3.5 cm of the TBP layer and butanol mixed in the top 5 cm of the aqueous layer in about 5 minutes at typical gas flow rates for the oxidation reactions. Based on the results of bench-scale reaction experiments [1], these rates are sufficient to replenish water lost by evaporation at evaporator temperatures. When just the top TBP layer was sparged, mixing was about 100 times slower. Bubble size did not have an appreciable effect on the rate of transfer.

During the transfer of water from the aqueous aluminum nitrate solution and the transfer of butanol from TBP, the concentration leveled off short of saturation. The partial saturation of TBP with water from the aluminum nitrate solution probably occurred because the aqueous solution became saturated with the aluminum nitrate salt at the interface. The partial saturation of butanol in the aqueous layer was attributed to poor mixing in the bottom portion of that layer.

A mass transfer coefficient was derived for use in modeling oxidation experiments. This coefficient is directly proportional to the superficial gas velocity (the volumetric flow rate divided by the cross-sectional area) and inversely proportional to the liquid layer depth.

3.0 Experimental Design and Apparatus

The mass transfer experiments measured rates of transfer of water and butanol between immiscible aqueous and TBP layers with air sparging of one or both layers. Three sets of experiments were performed. The first set measured the rates of transfer of water from a layer of deionized water or an aqueous aluminum nitrate solution into a TBP layer with sparging of both layers. The second set measured water transfer rates from an aqueous aluminum nitrate solution into TBP with sparging of just the top TBP layer. Finally, a third set of experiments measured butanol transfer rates from a TBP layer into deionized water with sparging of both layers. Nitric acid was not added to the aqueous phase because it reacted with TBP to produce nitrous oxides that interferred with the water concentration measurements. Table 1 lists conditions for each experiment.

The experimental apparatus was comprised of a modified 250-mL graduated cylinder with an inside diameter of 3.59 cm. It was joined to a specially fabricated glass cover by a ground glass joint. An air sparger was inserted through the cover, which also had a port for a sampling tube. In addition to the cover, the apparatus had an angled side port for insertion of the fiber optic probe, an air vent, and two additional side ports with stopcock valves, which were used for drainage. The apparatus was placed in a stirred constant temperature bath. Figure 1 depicts the apparatus configuration for the measurement of water transfer rates with sparging of both layers.

A peristaltic pump supplied sparge air, which was metered by a rotameter. The sparge air was introduced through either a thin plastic tube or through a 40-60 micron glass frit sparger. For sparging of both layers, the air discharge was located about 3 cm from the bottom of the aqueous layer, and for sparging of just the TBP layer, the discharge was about 1.5 cm above the aqueous-TBP interface.

To determine how the mass transfer rate varied with the sparge velocity, three sparge rates were used: 0.6, 1.5, and 3.0 $mL/cm^2/min$. All three rates are less than the flow rate of 4.5 $mL/cm^2/min$ measured during oxidation reactions conducted at 105°C. [1]

Mass transfer rates were measured using an online fiber-optic spectrophotometry technique developed by SRTC/Analytical Development [2]. Fiber optic transflectance probes were connected by fiber optic cables to spectrophotometers that measured light absorbance in the near infrared range. Concentrations of water in TBP and butanol in aqueous solutions were correlated with light absorbance due to vibrational overtones in -OH and -CH bonds.

The fiber optic probes were cylindrical, with a length of 5.0 cm and a diameter of 1.3 cm. Light absorbance was measured across a gap located at the end of each probe. The pathlength of this gap was 1.85 cm for the measurement of water concentrations in TBP and 1.35 cm for the measurement of butanol concentrations in the aqueous phase. To measure the rate of transfer of water from the aqueous layer into the TBP layer, the probe was placed so that the measurement path was centered halfway between the aqueous-TBP interface and the top surface of the TBP layer. The probe was connected to an EG&G Model 1235 spectrophotometer. To measure the rate of transfer of butanol from the TBP layer into the aqueous layer, the probe was placed so that the measurement path was

centered halfway between the bottom of the aqueous layer and the aqueous-TBP interface. For these measurements, the probe was connected to an HP Model 8452A-NIR spectrophotometer.

Each measurement was made by comparing a spectral density function with a standard density function for TBP with no water added (the butanol reagent contained up to 1% water by volume) or for water with no butanol. The spectral density functions were integrated electronically; the integration intervals were 7 seconds for the EG%G spectrophotometer and 4 seconds for the HP spectrophotometer. The spectrophotometric data was collected, integrated, converted to concentration units using regressions of calibration data, and stored in computer files using codes developed by SRTC/Analytical Development. Both meters were calibrated using standard solutions of known composition.

4.0 Description of Experiments

At the beginning of each experiment, 100 mL of aqueous solution and 70 mL of 99% TBP were added to the apparatus. These volumes gave an aqueous layer depth of about 10 cm and a TBP layer depth of about 7 cm. The apparatus was then placed in the constant temperature bath for about one hour. The temperature bath was kept at 80°C for the water transfer experiments and at 70°C for the butanol transfer experiments. The temperatures were limited to these values to minimize evaporation losses.

After the solutions were heated, air sparging was started, and the water or butanol concentration was recorded as a function of time until it approached a constant value. Changes in the level of the interface also were recorded, but this information was not used in the analysis of results. Instead, the mass transfer rate calculations were based on concentration measurements.

The plastic tube sparger generated bubbles about 0.3 cm in diameter, and the glass frit sparger produced bubbles less than a millimeter in diameter. The larger bubble size was comparable to that observed during oxidation experiments. Neither sparger could be centered in the apparatus, so the bubbles rose along one wall. The larger bubbles rose in a straight line to the top surface of the TBP layer, while the smaller bubbles became dispersed throughout the TBP layer once they crossed the aqueous-TBP interface. The column of bubbles from the frit sparger raised the level of the interface about 0.5 cm on one side of the apparatus. Subsequent analyses of results showed that this change in the interface level had little or no apparent effect on mass transfer rates, though.

The bubbles entrained drops of aqueous solution into the TBP layer. These drops eventually fell to the interface and deposited on top of the aqueous layer. The TBP phase was not entrained in the aqueous layer, because there was no bubble flow downward across the interface.

4.1 Experimental Uncertainties

There were significant uncertainties in the location of the transflectance probe, the sparge flow rate, the start time for sparging, the concentration measurement, and the solution temperature. The transflectance probe was centered of the layer of interest by eye; it is estimated that the uncertainty in this placement was about ± 0.2 cm. In addition, the interface between the two layers moved as much as 0.5 cm due to transfer of water or butanol during a typical test. Because the mass transfer analysis does not account for this movement, it is included as part of the experimental uncertainty. The sparge flow rate

was controlled within about ±5% at the lowest flow rate of 0.6 mL/cm^2/min and within about ±3% at the higher flow rates of 1.5 and 3.0 mL/cm^2/min. With the exception of the first test, a steady flow rate was established within approximately 10 seconds. The uncertainties in each concentration measurement were calculated electronically based on uncertainties in the probe calibration and variations in the spectral density function during the integration period. These uncertainties, which are tabulated along with the measurements, averaged between 1% and 10%. Finally, the solution temperature was controlled within ±5°C. To a minor extent, variations in the temperature affected both the transflectance probe calibration and the solubilities of water in TBP and of butanol in water.

5.0 Mass Transfer Model

Mass transfer rates were analyzed using an axial dispersion model. This model assumes that mixing in the vertical direction occurs primarily by displacement or entrainment of liquid by the bubbles. This mixing is modeled using Fick's law of diffusion, with a turbulent dispersion coefficient replacing the molecular diffusivity. Fick's law states that the mass transfer per unit surface area is the product of the turbulent axial dispersion coefficient and the gradient of the concentration:

$$N = -D\frac{\partial \bar{c}}{\partial x} \qquad (1)$$

where

$\bar{c}$ = local concentration, M or wt%
D = axial dispersion coefficient, cm^2/sec
N = mass flux due to axial dispersion, M-cm/sec or wt%-cm/sec
t = time after sparging begins, sec
x = distance from the aqueous-TBP interface, cm

The dispersion coefficient, which is a function of the liquid circulation velocity and either the diameter or the height of the mixing column, normally exceeds the molecular diffusivity by several orders of magnitude. To simplify the analysis, it is assumed that the dispersion coefficient is independent of position within each layer and does not vary with time.

To calculate the variation of concentration with time, Fick's law is combined with a one-dimensional mass balance, which takes the form

$$\frac{\partial \bar{c}}{\partial t} = -\frac{\partial N}{\partial x} \qquad (2)$$

The mass transfer rate calculations are based on the time required to reach an asymptotic final concentration. All concentration measurements were normalized with respect to the difference between the asymptotic final concentration and the initial concentration just before sparging began, using the following formula.

$$c = \frac{\bar{c} - \bar{c}_i}{\bar{c}_s - \bar{c}_i} \qquad (3)$$

where

c = dimensionless concentration
$\bar{c}_i$ = initial concentration, M or wt%
$\bar{c}_s$ = saturated concentration at the aqueous-TBP interface, M or wt%

In terms of this dimensionless concentration, the mass balance for the axial dispersion model is

$$D\frac{\partial^2 c}{\partial x^2} = \frac{\partial c}{\partial t} \tag{4}$$

where

D = axial dispersion coefficient, cm^2/sec
t = time after sparging begins, sec
x = distance from the aqueous-TBP interface, cm

This equation takes different boundary conditions for water transfer into the TBP layer and butanol transfer into the aqueous layer. The same model is used for mixing of water into the TBP layer for sparging of both layers and just the top TBP layer.

5.1 Model for Transfer of Water into TBP

With sparging of both layers, the controlling resistance to transfer of water across the aqueous-TBP interface is in the TBP layer. The reason is that very little mass is transferred in the aqueous phase, due to the low solubility of TBP in water. Instead, the interface moves downward as water is absorbed in the TBP layer. For this case, the interfacial condition is that the concentration of water remains constant at its saturation level in TBP. In other words,

$$c = 1 \text{ at } x = 0 \tag{5}$$

The boundary condition at the top surface of the TBP layer is that there is no mass transfer by dispersion. This gives

$$\frac{\partial c}{\partial x} = 0 \text{ at } x = h \tag{6}$$

Finally, the initial condition is

$$c = 0 \text{ for } t = 0,\ x > 0 \tag{7}$$

For this set of conditions, the solution is given by [3]

$$c = 1 - \frac{4}{\pi}\sum_{n=1}^{\infty}\frac{1}{2n-1}\sin\left(\frac{(2n-1)\pi x}{2h}\right)\exp\left(-\frac{(2n-1)^2\pi^2 Dt}{4h^2}\right) \tag{8}$$

At the center of the TBP layer, this reduces to

$$c = 1 - \frac{4}{\pi}\sum_{n=1}^{\infty}\frac{1}{2n-1}\sin\left(\frac{(2n-1)\pi}{4}\right)\exp\left(-\frac{(2n-1)^2\pi^2 Dt}{4h^2}\right) \qquad (9)$$

This analysis neglects the movement of the interface downward as water mixes in the TBP layer. This movement should have a secondary effect on the axial dispersion, primarily due to the displacement of the measurement location from the center of the TBP layer.

When just the TBP layer is sparged, the preceding analysis is still valid, albeit with a lower dispersion coefficient due to the reduction in mixing at the interface.

5.2 Model for Transfer of Butanol into Water

Transfer of butanol to the aqueous layer differs from transfer of water to the TBP layer in that there is no direct mixing by displacement or entrainment of TBP droplets in the aqueous layer. Instead, aqueous droplets mix in the aqueous phase and then redeposit at the aqueous-TBP interface. If it is assumed that these droplets become saturated in the TBP layer, a mass balance at the interface gives

$$-D\frac{\partial c}{\partial x} = -v_{droplet}(1-c) \text{ at } x = h \qquad (10)$$

If it is also assumed that the volumetric flow rate of aqueous droplets is equal to the volume displaced by the bubbles, then

$$v_{droplet} = v_{sg} \qquad (11)$$

and

$$-D\frac{\partial c}{\partial x} = -v_{sg}(1-c) \text{ at } x = h \qquad (12)$$

There are two possible boundary conditions at the bottom surface. Both derive from the requirement that there is no mass transfer at this surface. One condition sets the concentration gradient equal to zero, as was done for the TBP layer. This yields

$$\frac{\partial c}{\partial x} = 0 \text{ at } x=0 \qquad (13)$$

The other approach is to specify that the bottom concentration does not change with time. This condition implies that there is no mass transfer into or out of the bottom region. It is valid when the axial dispersion near the bottom surface is much less than in the bulk fluid. By setting the time dependent term in the mass balance (Equation 4) equal to zero, this boundary condition can be expressed by

$$\frac{\partial^2 c}{\partial x^2} = 0 \text{ at } x=0 \qquad (14)$$

With these boundary conditions, it is not convenient to solve the mass balance analytically. Instead, the problem was solved using a finite difference calculation.

The steady state solution of the mass balance with this boundary condition is a linear concentration profile of the form

$$c = \frac{xv_{sg}}{hv_{sg} + D} \tag{15}$$

6.0 Experimental Results

A dispersion coefficient was determined for each mass transfer experiment by graphically fitting a calculated concentration time profile to the measured data. The initial concentration, the asymptotic final concentration, and the dispersion coefficient each were varied to obtain the best possible fit.

Figures 2, 3, and 4 compare calculated profiles with measurements for transfer of water into the TBP layer at increasing sparge rates. In Figure 2, the starting time was adjusted to compensate for difficulties in establishing flow through the peristaltic pump, and a series of concentrations was corrected to account for the presence of a water droplet in the probe measurement volume, which temporarily increased the measured water concentration. With these corrections, the model agrees with the data reasonably well. The agreement between the model and the measurements is better in Figures 3 and 4. A comparison among these experiments shows that the rate of mixing goes up significantly as the sparge rate increases.

Figure 5 compares calculations with measurments for transfer of water into TBP using a glass frit sparger. The dispersion coefficient for this test is nearly equal to that for the test at the same sparge rate using the plastic tube (see Figure 2). This indicates that the mass transfer rate is independent of bubble size and depends only on the volumetric flow rate per unit area. Furthermore, it probably signifies that the primary mechanism by which the bubbles mix the liquid layer is either displacement or entrainment of surrounding fluid. If the bubbles transferred kinetic energy to the liquid, the mass transfer would be greater for the larger bubbles, which have a much greater rise velocity. This contention is supported by Joshi [4], who analyzed mixing in bubble columns. He stated that below a superficial gas velocity of 0.05 m/sec, there is little energy transfer between the bubbles and the liquid.

Figure 6 shows data for transfer of water from a 40 weight percent aluminum nitrate solution into TBP. The dispersion coefficient for this experiment is about 35% greater than for transfer of water from a pure water layer at the same sparge rate. This indicates that the mass transfer rates are not significantly lowered by large differences between the densities of the two layers. (The difference in the densities of the TBP layer and the density of the aluminum nitrate layer was about 0.4 gm/mL; by contrast, the difference in the densities of TBP and water is less that 0.05 gm/mL.)

Figures 7 and 8 depict mass transfer rates of water from a 40 weight percent aluminum nitrate solution into TBP with sparging of just the TBP layer. The dispersion coefficients for these tests are on the order of 1% of those for sparging of both layers. The order of magnitude of this change suggests that mass transfer in the TBP layer is limited by boundary layer effects at the aqueous-TBP interface. Although the dispersion

coefficients are quite low for these tests, they are still much greater than molecular diffusivities, which are typically about 1 x 10^{-5} cm^2/sec.

As the water concentrations in these two tests approached equilibrium, they exhibited different behaviors. In Figure 7, the concentration at first rose steadily, but later oscillated about an apparent equilibrium concentration of 0.92 M. In Figure 8, the concentration rose, briefly spiked, and then converged on a significantly higher final concentration of 1.35 M. The dispersion coefficient for Figure 7 was calculated based on the initial increase in concentration prior to the oscillations; an arbitrary maximum concentration of 1.2 M was used for this calculation. The apparently anomalous behavior subsequent to this initial increase was ignored. The dispersion coefficient for Figure 8 was computed using a final equilibrium concentration of 1.35 M.

Figures 9 and 10 compare calculated and measured rates of transfer of butanol into the aqueous phase. Figure 9 clearly shows a dichotomous behavior. The butanol concentration at first rises relatively rapidly to about half its saturation level of 6.5 wt% [5] and then more slowly. That the concentration levels off about halfway to saturation supports the contention that the mass transfer is governed by a steady state boundary condition at the bottom of the aqueous layer. As demonstrated previously, this boundary condition results in a linear profile, with a zero butanol concentration at the bottom and a concentration that approaches saturation at the aqueous-TBP interface. The measured concentration midway through the aqueous layer would be halfway between, or about half the saturation value. The subsequent rise in the butanol concentration most likely can be attributed to secondary mixing with a no mass transfer boundary condition replacing the steady state boundary condition at the bottom. With this new boundary condition, the aqueous layer would eventually become saturated with butanol. The dispersion coefficient for this secondary mixing is about one-third as large as for the initial mass transfer. This may indicate that the length scale for the secondary mixing was the diameter of the apparatus, whereas the initial length scale was the total height of the aqueous layer. (The depth of the aqueous layer was about three diameters.) Natural mixing cell lengths of about one diameter have been reported by Joshi. [4] In Figure 10, the measured butanol concentration also rises to about halfway to saturation, but subsequent secondary mixing is not as evident.

7.0 Correlation of Dispersion Coefficients

The dispersion coefficients were correlated as functions of the superficial gas velocity and the liquid layer depth. Table 2 lists the superficial gas velocity, the layer depth, and the calculated dispersion coefficient for each experiment.

As Table 2 indicates, when both layers were sparged, the dispersion coefficients for transfer of water into TBP from pure water and an aqueous salt solution and for transfer of butanol from TBP into water were not significantly different. Therefore, a single correlation was used for these coefficients. This correlation takes the form

$$D_{2-layer} = 0.621h\left(v_{sg} - 0.0084\right) \qquad (16)$$

where

$D_{2-layer}$ = dispersion coefficient for two-layer sparging, cm^2/sec

The dispersion coefficients for sparging of just the TBP layer were significantly lower. The correlation for single-layer sparging is

$$D_{1-layer} = 0.0105h\left(v_{sg} - 0.00030\right) \qquad (17)$$

where

$D_{1-layer}$ = dispersion coefficient for sparging of just the TBP layer, cm^2/sec

Figure 11 illustrates the correlation of the dispersion coefficients for two-layer sparging, and Figure 12 depicts the correlation of the dispersion coefficients for single-layer sparging. Both figures include 95% upper and lower confidence bounds. There is a 95% probability that the correct correlation gives dispersion coefficients either less than the upper bound or greater than the lower bound, or a 90% probability that the correct correlation lies between the two confidence bounds. These confidence bounds were calculated as the root sum of squares of an estimated combined experimental and analytical error of 20% in determining individual dispersion coefficients and a statistical correlation error. The 20% relative error approximates the uncertainty in fitting each dispersion coefficient to the measured data; all measurement errors were significantly smaller than this. The statistical correlation error represents the 95% confidence bounds for the two-layer correlation of dispersion coefficients. (These correlation error bounds give limits for the correct correlation of the data. It is not implied that 90% of the data should lie within the bounds.) The same statistical bounds were used for the single-layer correlation, due to the lack of data for single-layer bubbling. The statistical error predominates at lower gas velocities, and the relative experimental and analytical error is more significant at higher velocities.

As Figures 11 and 12 show, both the two-layer and single-layer correlations predict that there is a minimum sparge velocity below which mass transfer is not enhanced. This minimum velocity may be an artifact of the linear correlation (i.e., the dispersion coefficient may really be proportional to the velocity to a power greater than one), or it may indicate that there is a minimum velocity required to transfer material across the aqueous-TBP interface. If it is an artifact and the dispersion coefficient is proportional to a higher power of the superficial velocity, extrapolation using these linear correlations will yield conservatively low dispersion coefficients.

7.1 Comparison of Results with Previous Work

A literature search did not produce any correlation for mixing due to bubbling from a chemical reaction. The closest analog for which correlations are available is a bubble column in which gas is sparged upward through a stagnant liquid layer. Most such correlations are empirically-based and are expressed in terms of the gas superficial velocity and the diameter of the column. Such correlations are not appropriate for the nitric acid-TBP system because the column diameter cannot be used as a scaling factor.

One correlation that has a theoretical basis and relates the dispersion coefficient to the liquid layer depth is that of Joshi [4], which was mentioned previously. The Joshi correlation is based on a balance between the kinetic energies of the bubbles and the liquid-phase circulation generated by the bubble motion. It gives the dispersion coefficient in terms of the liquid circulation velocity and a transfer unit height:

$$D = 0.3H_T V_C \quad (18)$$

where

H_T = height of a mixing cell or a mass transfer unit
V_C = liquid circulation velocity

The Joshi correlation corresponds to Equations 16 and 17, if the layer depth equals the mixing cell height and the liquid circulation velocity equals twice the superficial bubble velocity. (The liquid must circulate up and down so the effective cross-sectional area for the liquid circulation is half that for the bubble flow, and the circulation velocity of the liquid displaced by the bubbles is twice the superficial bubble velocity.)

The problem with this analogy, as explained previously, is that the measurements in the present study were performed at low gas velocities, where Joshi states that the energy balance approach does not apply. According to Joshi, when the gas superficial velocity falls below about 5 cm/sec, the bubbles rise at their terminal velocity and energy transfer to the liquid phase occurs only at the gas-liquid interface.

A review of Joshi's analysis follows. This review shows where the energy balance approach breaks down and where, by implication, bubble-induced mixing occurs solely by volumetric displacement of the liquid phase.

As Equation 18 indicates, Joshi's correlation requires the estimation of a liquid circulation velocity . This velocity is obtained by setting the rate of transfer of energy from the bubbles to the solution to the power contained in the liquid circulation within each layer:

$$\dot{E}_b = \dot{E}_l \quad (19)$$

where

$\dot{E}_b$ = rate of transfer of energy from the bubbles to the liquid, watt
$\dot{E}_l$ = rate of dissipation of energy by the liquid, watt

The rate of transfer of energy from the bubbles is the product of the bubble velocity and the drag force of the bubbles:

$$\dot{E}_b = 0.5 c_d \rho_s v_b^2 A_b v_{sg} \quad (20)$$

where

A_b = cross-sectional area occupied by bubbles, cm^2
c_d = bubble flow drag coefficient
v_b = bubble velocity, cm/sec
ρ_s = liquid density, cm^3/sec

The bubble velocity is related to the gas superficial velocity by

$$v_b = \frac{v_{sg}}{\varepsilon} \tag{21}$$

where

ε = fraction of cross-sectional area occupied by bubbles

and the bubble flow area is related to the total cross-sectional area by

$$A_b = \varepsilon A \tag{22}$$

where

A = total cross-sectional area, cm^2

Therefore,

$$\dot{E}_b = \frac{0.5 c_d \rho_s v_{sg}^3 A}{\varepsilon} \tag{23}$$

To solve the preceding equations for the liquid circulation velocity, an additional relation is needed for the bubble volume fraction, ε. Measurements in bubble columns show that gas volume fractions are less than or equal to 0.06 times the gas superficial velocity in cm/sec [6]. Assuming that this relation holds for bubbles generated by reaction,

$$\varepsilon = B v_{sg} \tag{24}$$

where B = 0.06 sec/cm.

Substituting,

$$\dot{E}_b = \frac{0.5 c_d \rho_s v_{sg}^2 A}{B} \tag{25}$$

The power due to liquid recirculation was calculated by Joshi [4]. For shallow liquid layers, this power approached the value:

$$\dot{E}_l = \frac{15}{64} \rho_s v_c^3 A \tag{26}$$

For deep liquid layers, the recirculation power was

$$\dot{E}_l = \frac{26.3}{64} \rho_s v_c^3 A \tag{27}$$

The circulation velocity, v_c, is obtained by substituting Equations 25 and 26 or 27 in Equation 19. This gives

$$v_c = \sqrt[3]{\frac{32 c_d v_{sg}^2}{15B}} \tag{28}$$

for shallow layers and

$$v_c = \sqrt[3]{\frac{32 c_d v_{sg}^2}{26.3B}} \tag{29}$$

for deep layers.

Joshi [4] states that the dispersion coefficient is proportional to the product of this circulation velocity and the bubble column diameter:

$$D = 0.24 d_t v_c \tag{30}$$

He also states that a bubble column can be considered to be a number of mixing cells in series, with an equivalent mixing cell height of 0.8 column diameters. If either the aqueous or the organic layer is assumed to represent one mixing cell, then

$$h = 0.8 d_t \tag{31}$$

and

$$D = 0.3 h v_c \tag{32}$$

Finally, substitution of Equations 28 and 29 in Equation 32 yields expressions for the dispersion coefficient in terms of the gas superficial velocity, the layer thickness, and liquid properties. For shallow layers,

$$D = 0.3h \sqrt[3]{\frac{32 c_d v_{sg}^2}{15B}} \tag{33}$$

and, for deep layers,

$$D = 0.3h \sqrt[3]{\frac{32 c_d v_{sg}^2}{26.3B}} \tag{34}$$

Figure 13 compares the modified Joshi correlations for mixing in deep and shallow layers with the two-layer dispersion correlation from this study. This figure shows that, for deep layers, the correlation from this study gives a smaller dispersion coefficient below a superficial gas velocity of about 2.2 cm/sec, and the Joshi correlation yields a smaller dispersion coefficient above 2.2 cm/sec. For mixing in shallow layers, the correlation from this study gives a smaller coefficient below 4 cm/sec, and the Joshi correlation gives a smaller coefficient above 4 cm/sec. In either case, a conservative approach dictates that

the smaller of the two dispersion coefficients should be used. This approach in effect argues that at lower bubbling rates mixing is limited to simple volumetric displacement of the liquid phase, while at higher bubbling rates the bubbles interact with the liquid phase through drag forces.

8.0 Derivation of Mass Transfer Coefficient

The model of the TBP-nitric oxidation reactions is based on the bulk concentrations of the constituents in each phase and the equilibrium concentrations at the interface. Consequently, the dispersion coefficient must be converted to a bulk mass transfer coefficient, defined by the following equation.

$$\frac{dc_b}{dt} = k_x\left(1 - c_b\right) \tag{35}$$

where

c_b = bulk average concentration in the layer
k_x = bulk mass transfer coefficient

The bulk concentration is calculated from:

$$c_b = \frac{1}{h}\int_{x=0}^{h}(c)dh \tag{36}$$

When the initial concentration is zero and the interfacial concentration remains at the saturation point, this integral reduces to [7]:

$$c_b = \frac{8}{\pi^2}\sum_{n=1}^{\infty}\frac{1}{(2n-1)^2}\left(1 - \exp\left(-\frac{(2n-1)^2\pi^2 Dt}{4h^2}\right)\right) \tag{37}$$

An approximation can be obtained by integrating

$$\frac{dc_b}{dt} = \frac{4D\left(1 - c_b^4\right)}{\pi h^2 c_b} \tag{38}$$

Integration gives:

$$c_b = \sqrt{\frac{1 - \exp\left(-\frac{8Dt}{\pi h^2}\right)}{1 + \exp\left(-\frac{8Dt}{\pi h^2}\right)}} \tag{39}$$

Figure 14 shows the approximation given by Equation 39 agrees with the exact solution given by Equation 37 over the entire range of bulk concentrations.

Finally, factoring of Equation 38 and substitution of Equation 35 yields an expression for the mass transfer coefficient:

$$k_x = \frac{4D}{\pi h^2}\frac{1}{c_b}\left(1+c_b^2\right)\left(1+c_b\right) \qquad (40)$$

As $c_b \rightarrow 1$, the mass transfer coefficient has a minimum value given by

$$k_x = \frac{4.59D}{h^2} \qquad (41)$$

The preceding equations for k_x apply when the rate of mass transfer is much greater than the rate of disappearance of water due to reaction and evaporation. Based on the dispersion coefficients calculated in this study and the Smith et al. analysis of TBP-nitric acid oxidation reactions [1], this appears to be true.

9.0 Conclusions and Recommendations

The conclusions of this study are:

- For conditions observed in two-layer calorimetric experiments, the mass transfer due to bubbling is sufficient to replenish water and butanol lost by reaction.
- The dispersion coefficient is proportional to the superficial bubbling velocity and the liquid layer depth.
- The dispersion coefficient is independent of bubble size.
- The dispersion coefficients for water mixing in TBP and butanol mixing in water are approximately equal.
- The dispersion coefficient for bubbling in the TBP layer only is about 1% of the dispersion coefficient for bubbling in both layers.

The recommended expressions for the time rate of change of the bulk concentration, $\bar{c}_b$, and the bulk mass transfer coefficient, k_x, in dimensional terms, are:

$$\frac{d\bar{c}_b}{dt} = \frac{4D\left(\bar{c}_s^4 - \bar{c}_b^4\right)}{\pi h^2 \bar{c}_s^2 \bar{c}_b}$$

and

$$k_x = \frac{4D}{\pi h^2}\frac{1}{\bar{c}_s^2 \bar{c}_b}\left(\bar{c}_s^2 + \bar{c}_b^2\right)\left(\bar{c}_s + \bar{c}_b\right)$$

There are two recommended correlations for the axial dispersion coefficient in this equation. For bubbling in the aqueous layer (and necessarily in the TBP layer), the recommended correlation is

$$D_{2-layer} = 0.621h\left(v_{sg} - 0.0084\right)$$

For bubbling in just the TBP layer, the recommended correlation is

$$D_{1-layer} = 0.0105h\left(v_{sg} - 0.00030\right)$$

These correlations are estimated to be accurate within about ± 20% at superficial bubble velocities above 0.05 cm/sec. They should not be used at superficial bubble velocities above 2.2 cm/sec, where they would overestimate the amount of mixing.

10.0 Acknowledgments

The assistance of J. R. Smith, W. S. Cavin, P. E. O'Rourke, and T. B. Garbutt is appreciated. J. R. Smith and W. S. Cavin helped set up the experimental apparatus and assisted in conducting the mixing tests. P. E. O'Rourke of SRTC/Analytical Development developed spectrophotometric methods for measuring water and butanol concentrations and calibrated the spectrophotometers. T. B. Garbutt prepared samples for these calibrations.

11.0 References

1. J. R. Smith and W. S. Cavin, "Isothermal Heat Measurements of TBP-Nitric Acid Solutions (U)," WSRC-TR-94-XXX, September 16, 1994.

2. D. R. Van Hare, P. E. O'Rourke, W. S. Prather, M. B. Bowers, and M. J. Hovanec, "Online Fiber-Optic Spectrophotometry," DP-MS-88-186, February, 1989.

3. R. M. Barrer, Diffusion in and through Solids, Cambridge University Press, Cambridge (1951), p. 15.

4. J. B. Joshi, "Axial Mixing in Multiphase Contactors - A Unified Correlation," Trans. I. Chem. E., 58, 1980, pp. 155-165.

5. E. W. Washburn, ed., International Critical Tables of Numerical Data, Physics, Chemistry and Technology, Volume III, 1st ed., McGraw-Hill, New York (1928), p. 388.

6. Deckwer, W.-D., Burckhart, R., and Zoll, G., "Mixing and Mass Transfer in Tall Bubble Columns," Chem. Eng. Sci., 29, 1974, pp. 2177-2188.

7. R. M. Barrer, Diffusion in and through Solids, Cambridge University Press, Cambridge (1951), p. 17.

Table 1. Conditions for Mass Transfer Experiments

Expt. No.	Aqueous Phase	Organic Phase	Sparger	Sparged Layers	Sparge Rate ($mL/cm^2/min$)	Temp. (°C)
1	Deionized water	99% TBP	Tube	Both	0.6	80
2	Deionized water	99% TBP	Tube	Both	1.5	80
3	Deionized water	99% TBP	Tube	Both	3.0	80
4	Deionized water	99% TBP	Frit	Both	0.6	80
5	Aq. $Al(NO_3)_3$	99% TBP	Tube	Both	0.6	80
6	Aq. $Al(NO_3)_3$	99% TBP	Tube	TBP	1.5	80
7	Aq. $Al(NO_3)_3$	99% TBP	Tube	TBP	3.0	80
8	Deionized water	50% TBP sat'd w/H_2O, 50% C_4H_9OH	Tube	Both	0.6	70
9	Deionized water	50% TBP sat'd w/H_2O, 50% C_4H_9OH	Tube	Both	1.5	70

Table 2. Results of Mass Transfer Experiments

Expt. No.	Liquid Layer Depth (cm)	Superficial Gas Velocity* (cm/sec)	Dispersion Coefficient (cm^2/sec)
1	4.424	0.0196	0.03
2	7.038	0.0477	0.14
3	6.937	0.0937	0.36
4	7.038	0.0196	0.028
5	6.033	0.0196	0.04
6	7.038	0.0477	0.0014
7	7.038	0.0937	0.0048
8	10.054	0.0151	0.03**
9	10.054	0.0367	0.085**

* The superficial gas velocity accounts for both air and vapor from the solution. The bubbles were assumed to be in equilibrium with water at the test temperature. The vapor pressure was assumed to be 355.1 mm Hg at 80°C and 233.7 mm Hg at 70°C.

** These are the initial dispersion coefficients. The apparent dispersion coefficient for Experiment 8 later dropped to 0.01 cm^2/sec, and the apparent dispersion coefficient for Experiment 9 fell to 0.0283 cm^2/sec.

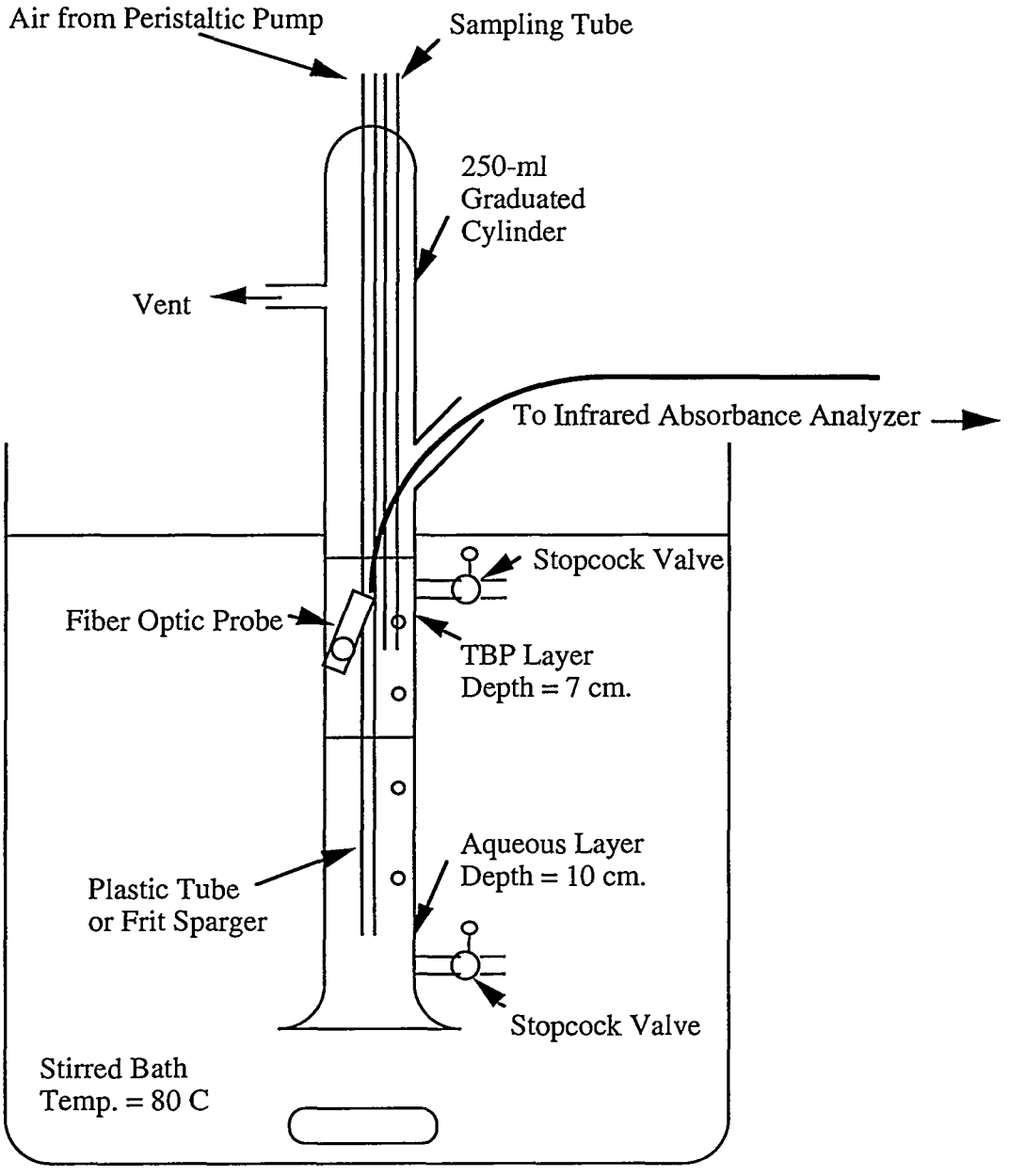

Figure 1. Test Apparatus for Measuring Rate of Mass Transfer of Water into TBP

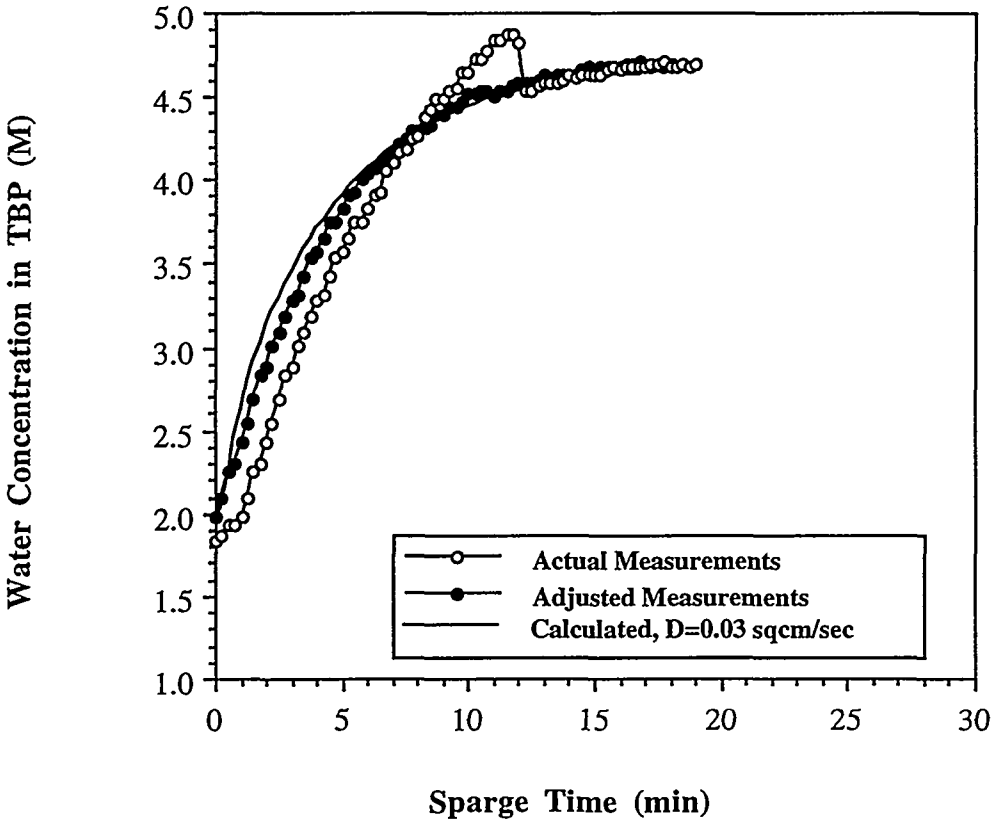

Figure 2. Mixing of Water in TBP at 80°C with a Sparge Rate of 0.6 ml/min/cm^2, Using a Sparge Tube

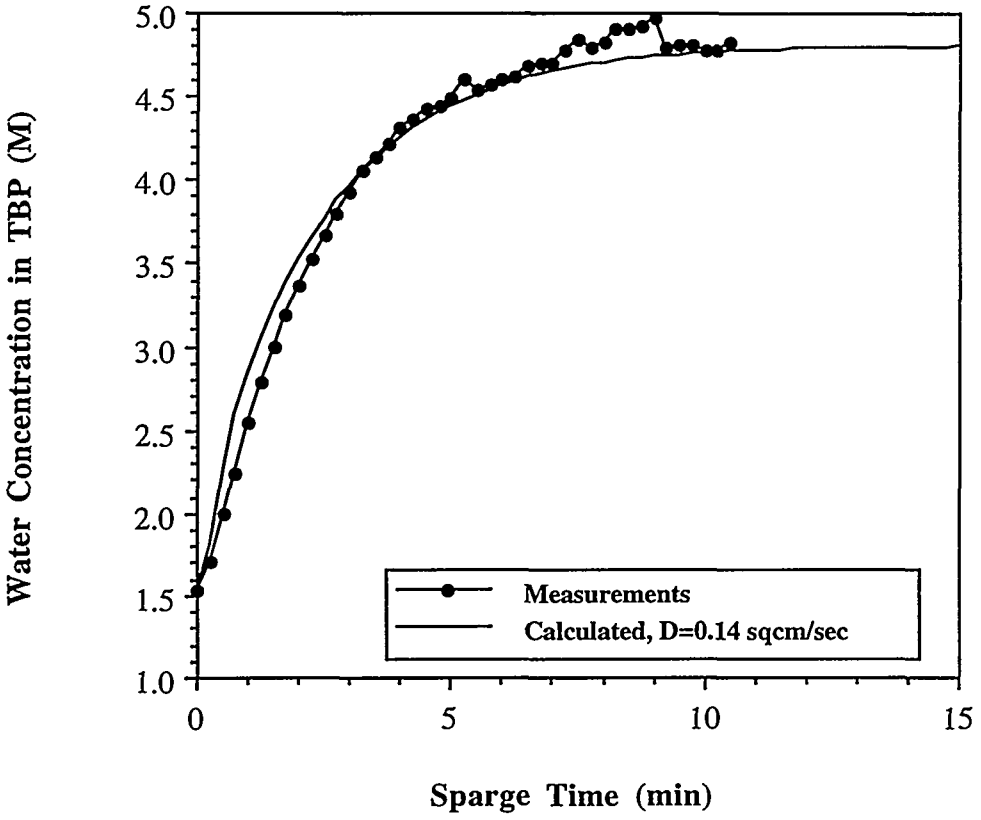

Figure 3. Mixing of Water in TBP at 80°C with a Sparge Rate of 1.5 ml/min/cm^2, Using a Sparge Tube

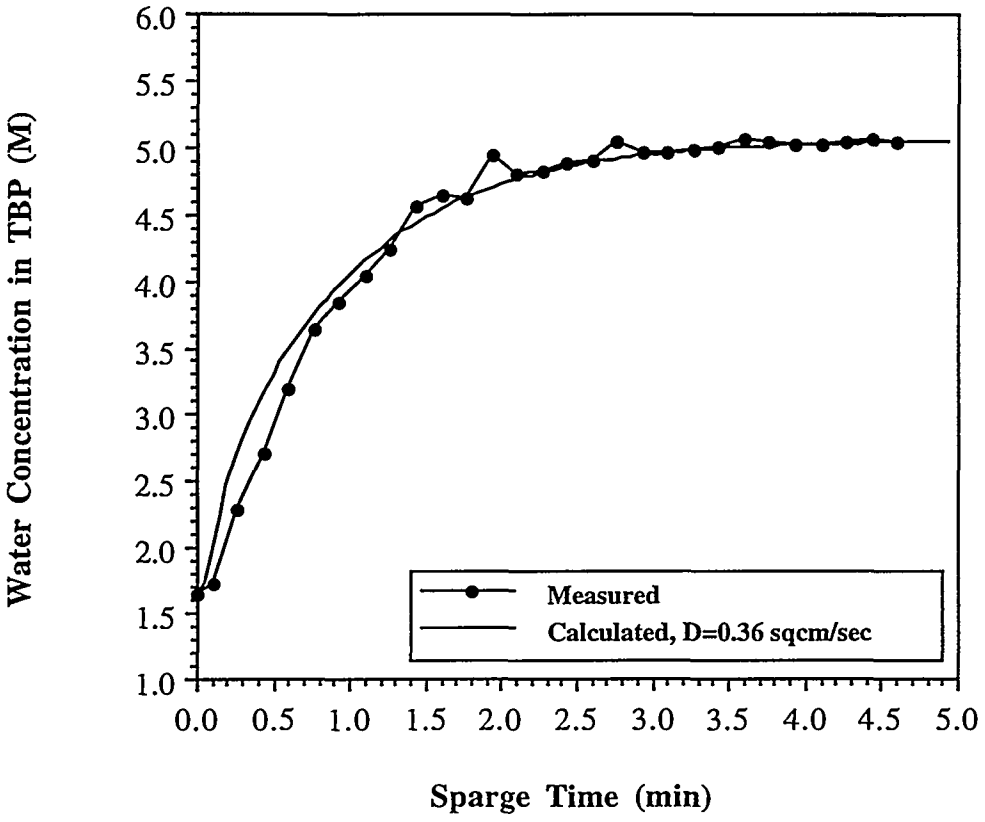

Figure 4. Mixing of Water in TBP at 80°C with a Sparge Rate of 3.0 ml/min/cm^2, Using a Sparge Tube

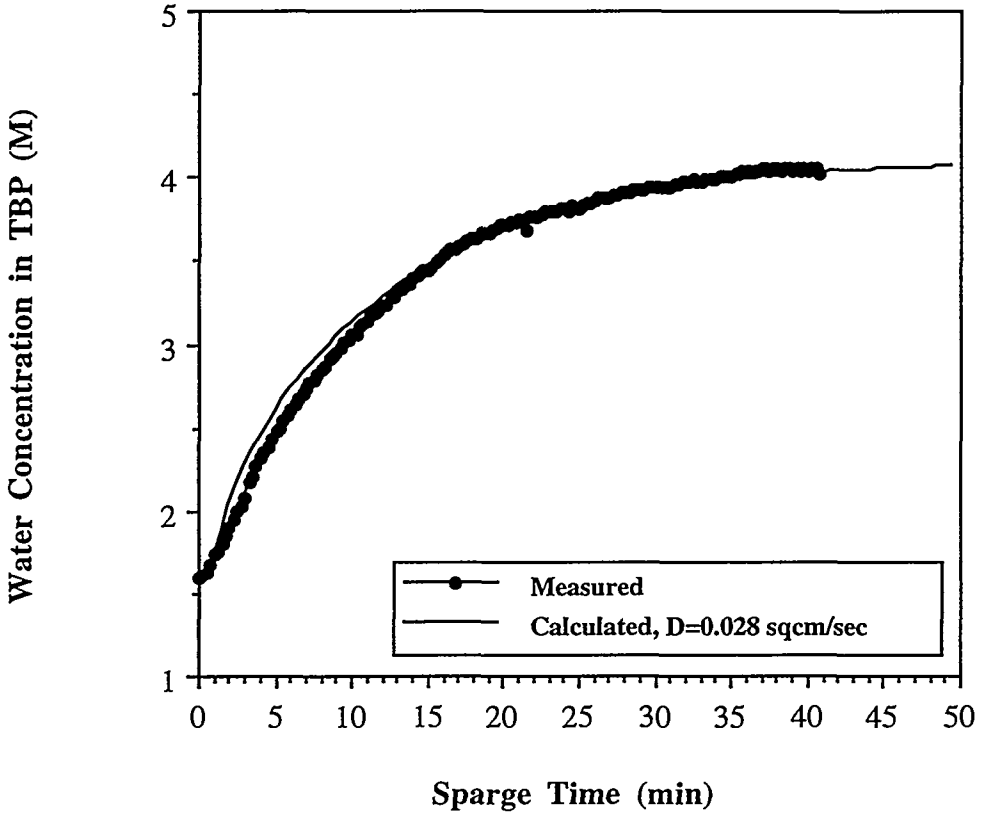

Figure 5. Mixing of Water in TBP at 80°C with a Sparge Rate of 0.6 ml/min/cm^2, Using a Frit Sparger

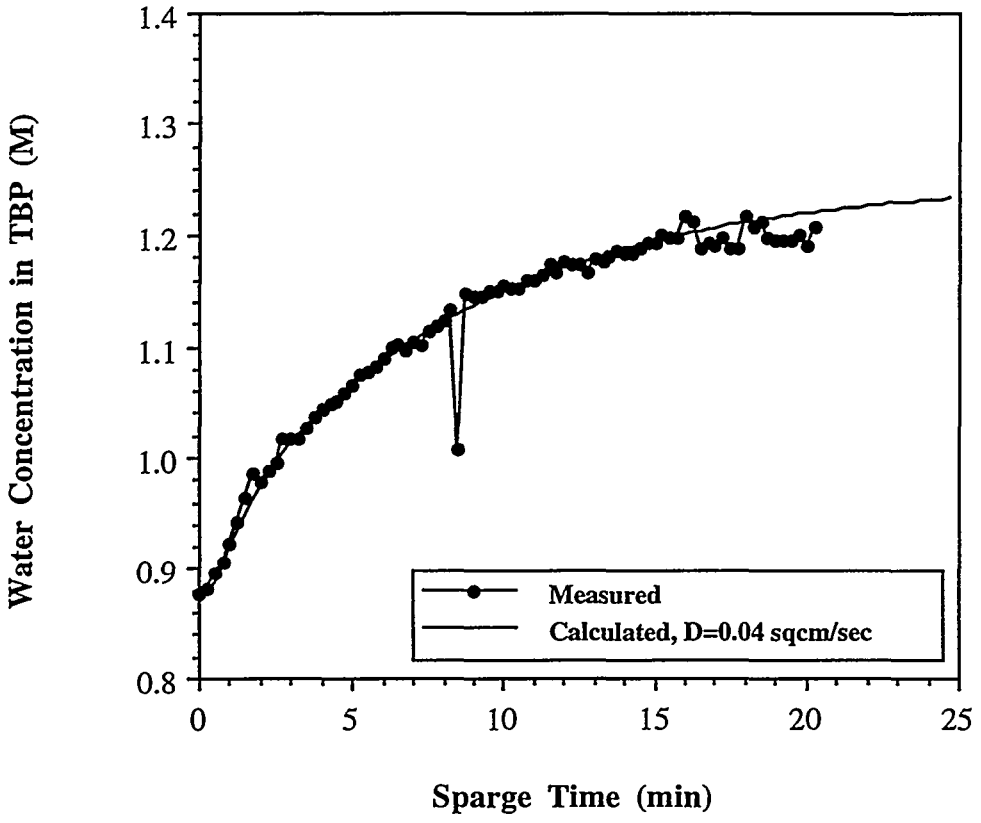

Figure 6. Mixing of Aqueous Al(NO3)3 in TBP at 80°C with a Sparge Rate of 0.6 ml/min/cm^2, Using a Sparge Tube

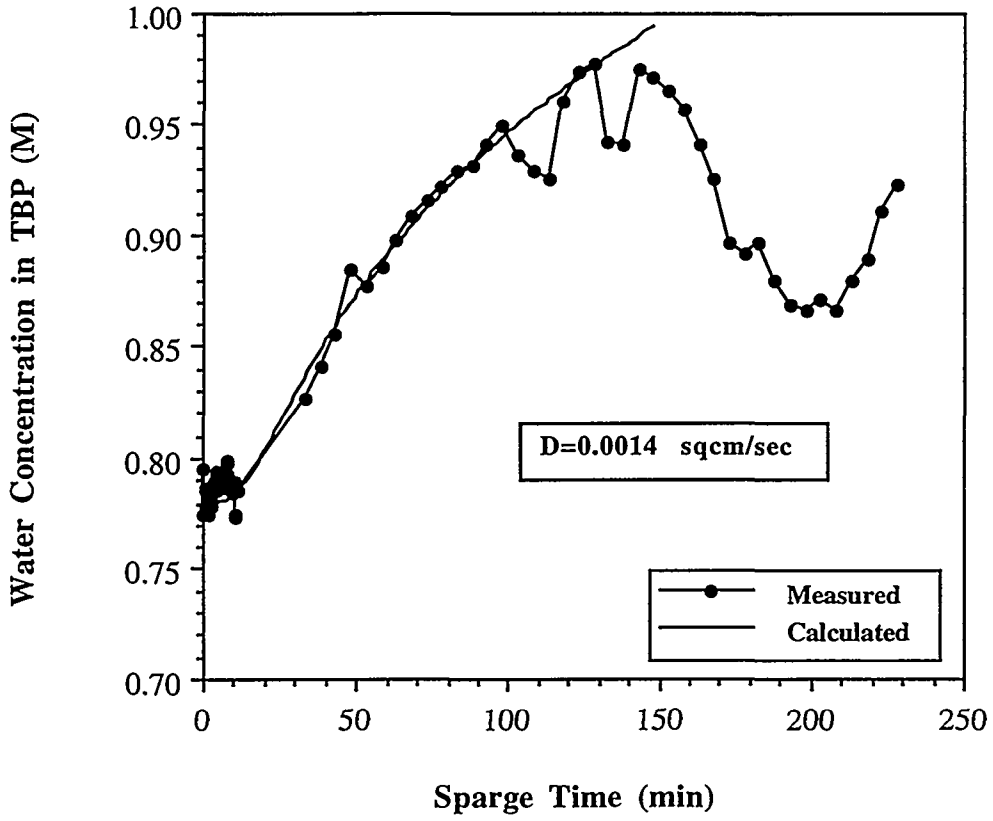

Figure 7. Mixing of Aqueous Al(NO3)3 in TBP at 80°C with a Sparge Rate of 1.5 ml/min/cm^2 in the TBP Layer Only, Using a Sparge Tube

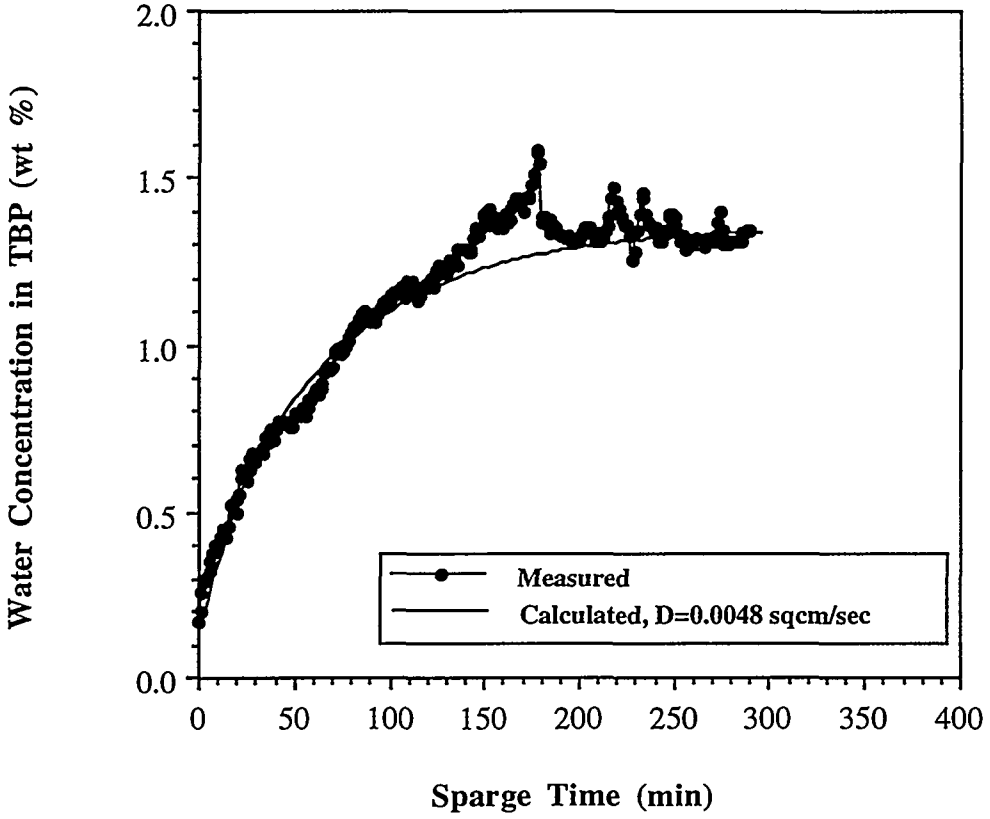

Figure 8. Mixing of Aqueous Al(NO3)3 in TBP at 80°C with a Sparge Rate of 3.0 ml/min/cm^2 in the TBP Layer Only, Using a Sparge Tube

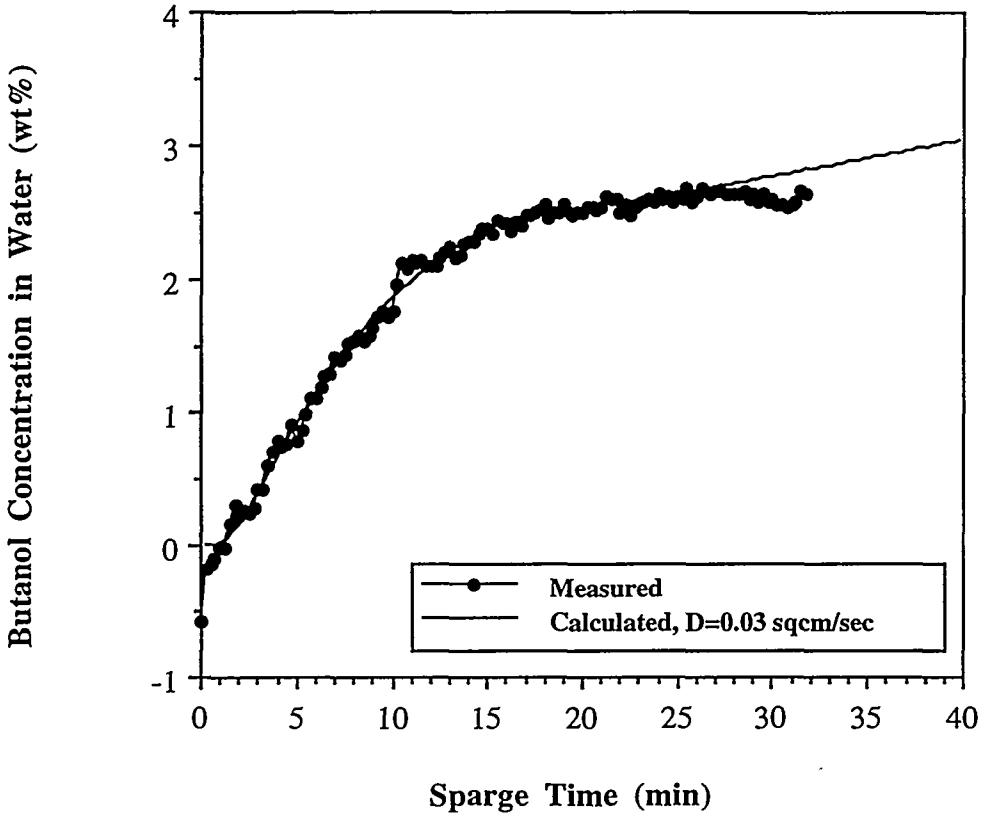

Figure 9. Mixing of Butanol in Water at 70°C with a Sparge Rate of 0.6 ml/min/cm^2, Using a Sparge Tube

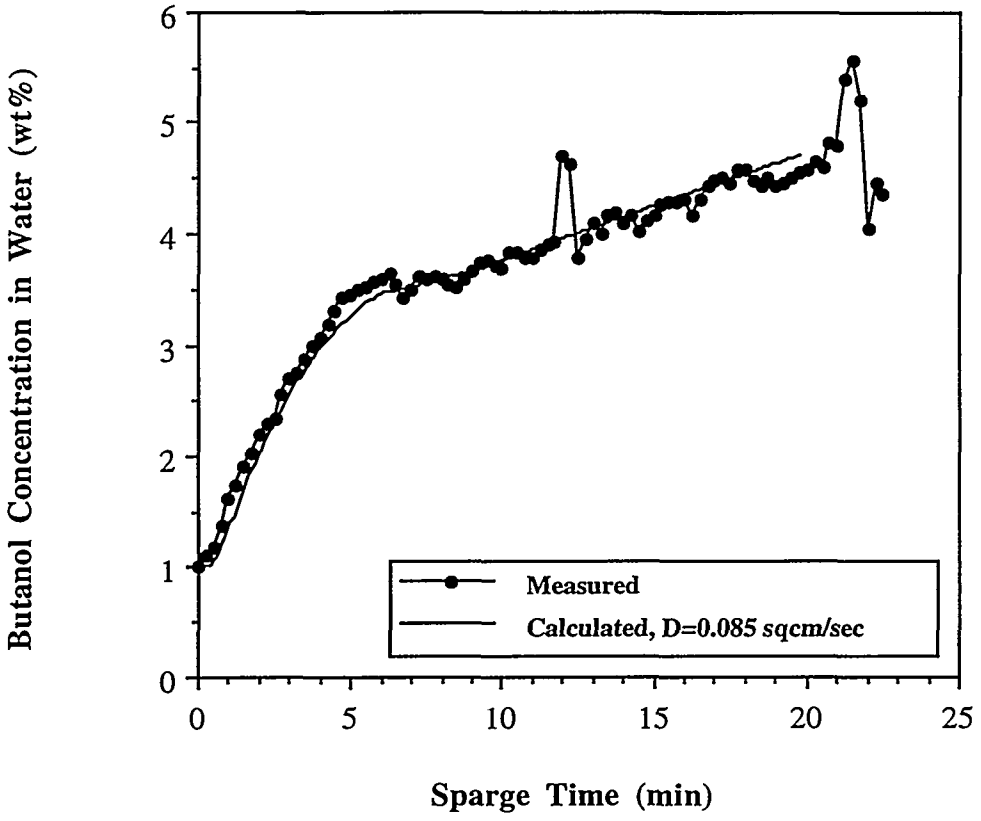

Figure 10. Mixing of Butanol in Water at 70°C with a Sparge Rate of 1.5 ml/min/cm^2, Using a Sparge Tube

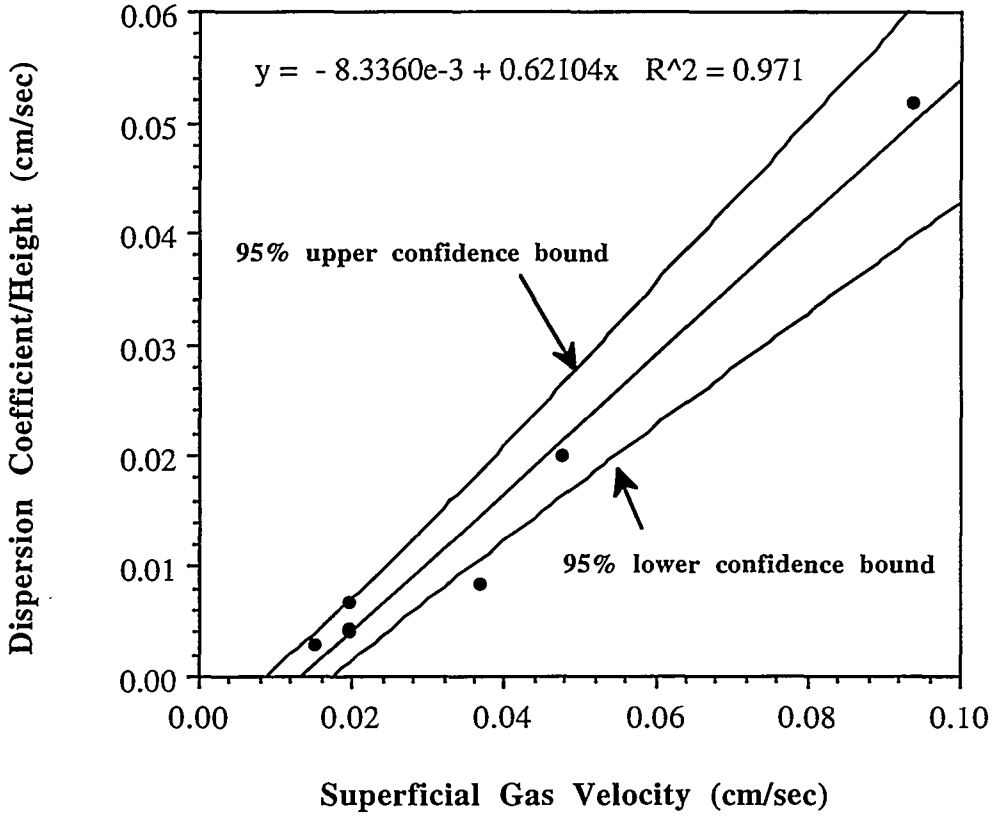

Figure 11. Dispersion Coefficient Correlation for Two-Layer Sparging

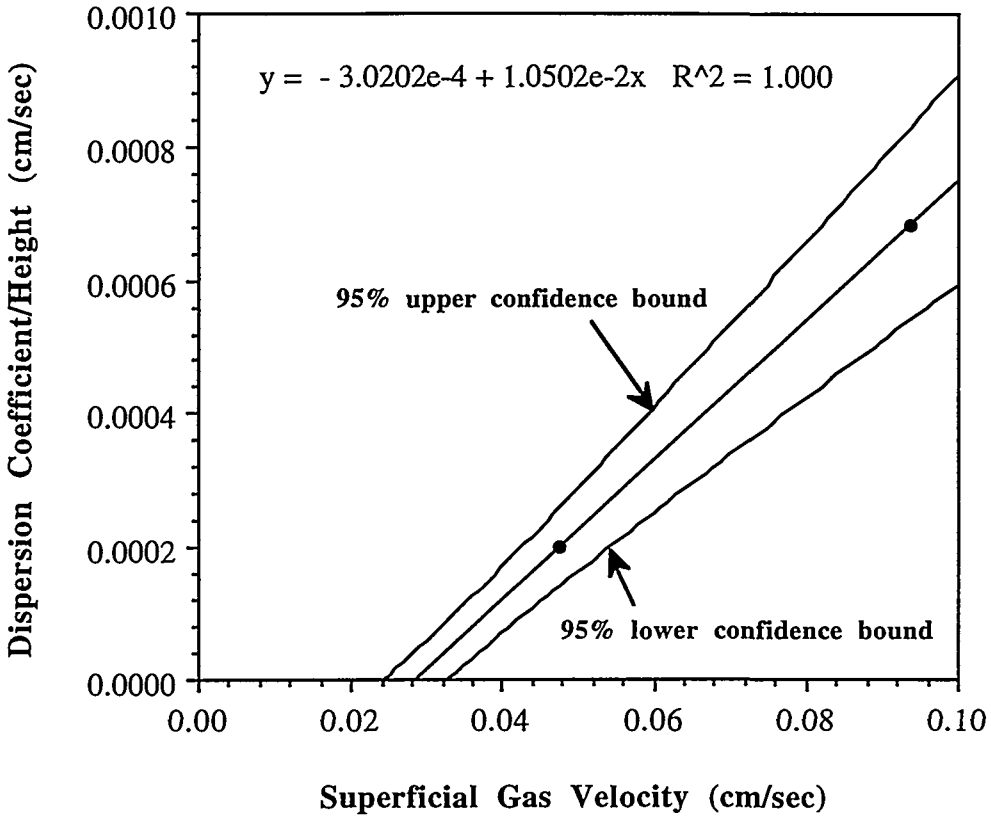

Figure 12. Dispersion Coefficient Correlation for TBP-Layer Sparging

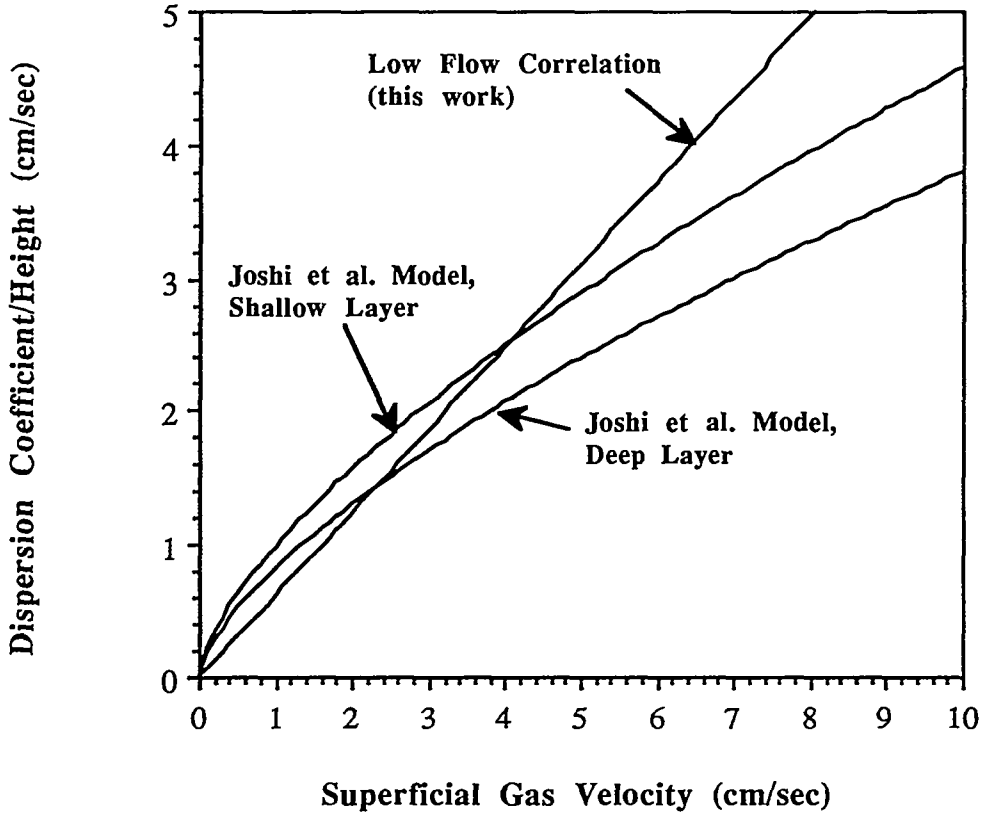

Figure 13. Comparison of Two-Layer Bubbling Dispersion Correlation with the Joshi et al. Recirculation Model

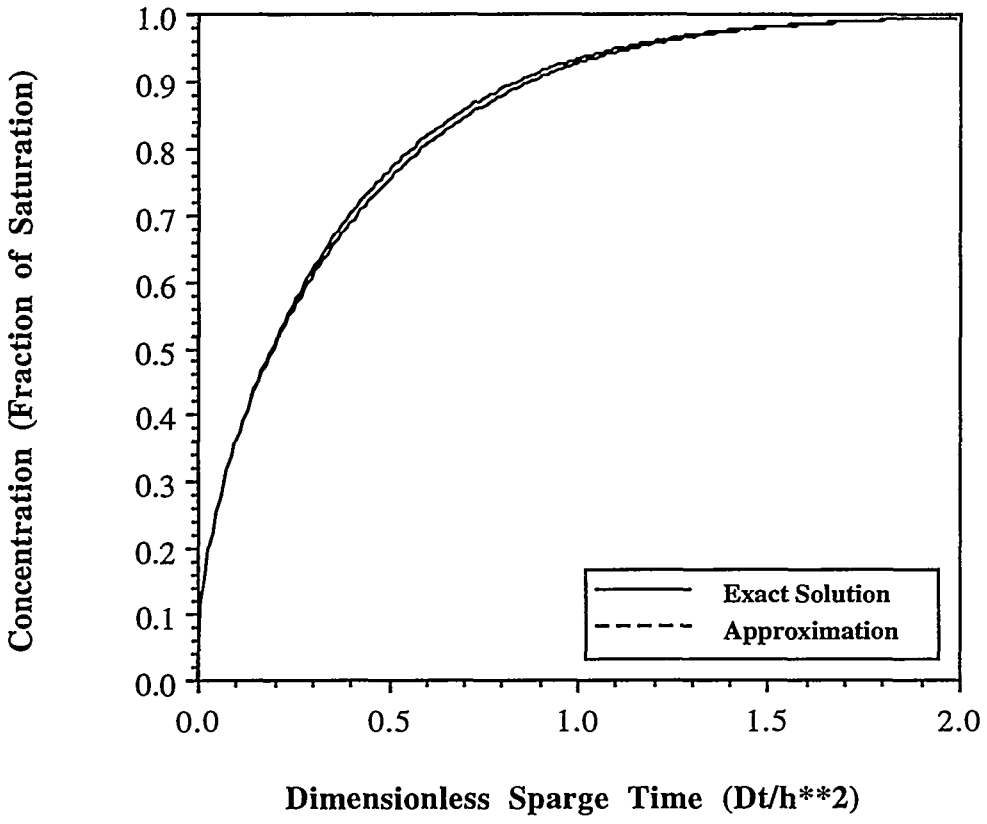

Figure 14. Comparison of Bulk Mass Transfer Approximation with Exact Solution of Diffusion Equation

WSRC INTERNAL DISTRIBUTION

Savannah River Technology Center

N. M. Askew, 773-A
W. S. Cavin, 773-A
F. R. Graham, 773-A
M. L. Hyder, 773-A
J. R. Knight, 773-A
J. E. Laurinat, 773-A
T. S. Rudisill, 773-A
J. R. Smith, 773-A
M. C. Thompson, 773-A
C. R. Wolfe, 773-A
SRTC Records, 773-52A

Savannah River Site

T. G. Campbell, 992W-1
M. L. Cowen, CCC-1
O. F. Ebra-Lima, 703-F
G. T. Geiger, 992W-1
D. F. Paddleford, 992W-1
J. R. Schornhorst, 992W-1